

## Article

# Research on the Optimization of Cutting Path of Cantilever Roadheader in Large Section Excavation

Chengjun Hu <sup>1,2</sup>, Yong Zhang <sup>1,\*</sup>, Rui Yu <sup>3,4</sup>, Xinqiu Fang <sup>3,\*</sup>, Ziyue Xu <sup>3</sup>, Lixin Wang <sup>2</sup> and Baofu Zhao <sup>2</sup>

<sup>1</sup> School of Energy and Mining Engineering, China University of Mining and Technology (Beijing), Beijing 100083, China; huchengjun@chinacoal.com

<sup>2</sup> China Coal Tianjin Underground Engineering Intelligence Research Institute, Tianjin 561000, China; wanglixin@chinacoal.com (L.W.); zhaobaofu@chinacoal.com (B.Z.)

<sup>3</sup> School of Mines, China University of Mining and Technology, Xuzhou 221116, China; lb19020006@cumt.edu.cn (R.Y.); ts20020060a31@cumt.edu.cn (Z.X.)

<sup>4</sup> Wangjialing Coal Mine, China Coal Huajin Group Co., Ltd., Yuncheng 043000, China

\* Correspondence: johnzy68@163.com (Y.Z.); fangxinqiu@cumt.edu.cn (X.F.); Tel.: +86-136-6110-8962 (Y.Z.); +86-139-1204-0883 (X.F.)

**Abstract:** Coal is an important resource for China and even for the whole world. With the improvement of mechanization, automation and intelligence of coal mining equipment in China, there has been an imbalance between the speed of mining and of excavating. Adopting efficient cutting paths is beneficial to improving roadway excavation efficiency and alleviating the imbalance between mining and excavation. In this paper, taking the 12307 belt roadway of Wangjialing Coal Mine as the research background, the geomechanical parameters and distribution characteristics of the surrounding rock were observed and studied, and the test results of in-situ stress, surrounding rock structure and surrounding rock strength were obtained. Based on the test results, a numerical model was established, and the stress and displacement distribution law of the surrounding rock of the roadway under different cutting paths were analyzed, and two optimal cutting paths were proposed based on the actual situation, and industrial tests were carried out. The test results show that using the “snake” cutting path from bottom to top, the roadway section forming effect is good, and a single cycle excavation takes 34 min, which verified the effectiveness of the cutting path design. On the basis of specific engineering geological conditions, excavation equipment and technology, combined with experimental testing, numerical simulation and other methods, the roadway excavation cutting path can be optimized, and the research results can provide a reference for the design of cutting paths for coal mine excavation roadways with the same geological conditions.

**Keywords:** cantilever roadheader; surrounding rock properties; numerical simulation; cutting path; large section roadway



**Citation:** Hu, C.; Zhang, Y.; Yu, R.; Fang, X.; Xu, Z.; Wang, L.; Zhao, B. Research on the Optimization of Cutting Path of Cantilever Roadheader in Large Section Excavation. *Sustainability* **2022**, *14*, 5345. <https://doi.org/10.3390/su14095345>

Academic Editors: Rajesh Kumar Jyothi, Fangtian Wang, Cun Zhang, Shiqi Liu and Erhu Bai

Received: 1 April 2022

Accepted: 26 April 2022

Published: 28 April 2022

**Publisher's Note:** MDPI stays neutral with regard to jurisdictional claims in published maps and institutional affiliations.



**Copyright:** © 2022 by the authors. Licensee MDPI, Basel, Switzerland. This article is an open access article distributed under the terms and conditions of the Creative Commons Attribution (CC BY) license (<https://creativecommons.org/licenses/by/4.0/>).

## 1. Introduction

Coal is an indispensable and important energy source for global economic development, accounting for about 30% of the world's total energy consumption and 70% of China's total primary energy consumption [1]. In recent years, with the improvement of the level of mechanization, automation and intelligence of coal mining equipment in China, the mining speed and output of coal mines have greatly increased, while the excavation speed is far behind the mining speed. Improving the excavation speed is the key to efficient coal mining [2,3]. The coal roadway excavation project mainly includes the three major processes of cutting, support and transportation [4–6]. Optimizing these three processes and improving their efficiency is conducive to solving the imbalance between the mining speed and the excavation speed, which ensures the safe and efficient mining of coal.

In terms of excavation cutting, Menezes et al. used numerical simulation to establish a cutting model of a wedge cutter, and obtained the key between cutting force, shear stress,

depth of cut, cutting speed and cutting angle [7–9]. Bilgin et al. obtained the formula of cutting force and optimal specific energy consumption through cutting experiments with different cutting depths and different cutting distances [10]. Fowell and Deliac et al. studied the pick cutter, proposed the mechanism of pick cutting, and verified and evaluated it by a combination of laboratory tests and numerical simulations [11,12]. Acaroglu et al. analyzed the influence of different cutting head shapes and their combinations on the cutting stability of the roadheader, and found that under a constant cutting angle, the stability of the drilling process was the worst and the cutting torque of the spherical cutting head was the smallest [13–15]. In addition, Slasani, Faradonbeh, Seker and many other scholars used instantaneous speed to judge the cutting performance of roadheaders, and proposed artificial intelligence technology models such as neural network, genetic algorithm and machine learning [16–19].

In terms of support, Wang et al. proposed a full-section anchor-grouting reinforcement technology, based on the numerical simulation results, and applied it to a coal roadway with broken and loose surrounding rock [20]. Cao et al. proposed a solution to the problems of sidewall collapse and floor heave in rock stratum roadway support using numerical software [21]. Yang et al. used the geological strength index to evaluate the properties of the surrounding rock of the roadway, and established the roadway model by using UDEC, which obtained the deformation characteristics of the roadway under different support methods, and the combined support scheme of anchor + net + cable + shotcrete + shell was proposed [22]. Li et al. proposed the soft rock roadway support technology under high stress.

After decades of development, the excavation equipment has perfectly integrated transportation and excavation cutting, which has reached a relatively mature stage. The current supporting equipment and processes for excavating mainly include the matching technology of the cantilever roadheader and the bolt drilling rig, the matching technology of the continuous miner and the bolting trolley, and the matching technology of the integrated drilling and anchoring unit [23–25]. Coal loading and transportation are carried out at the same time as excavation and cutting, realizing the parallel operation of excavation and cutting, and transportation.

Although predecessors have carried out much research on excavation cutting, support and transportation, they mainly focus on cutting performance and support methods, while less research has been done on the cutting path of roadheaders. The cutting path can improve the driving efficiency and stability of the roadheader. In this paper, the 12307 belt roadway in Wangjialing Coal Mine was taken as the engineering background; by means of field test, numerical simulation and industrial test, we obtained the geomechanical parameters and distribution characteristics of the surrounding rock of the 12307 belt roadway, studied the deformation law of the surrounding rock under different cutting paths, and designed the cutting path in combination with the actual situation and simulation results. The industrial test shows that after adopting the optimal cutting path, the roadway forming effect is good, the single cycle excavation takes 34 min and the excavation efficiency is high.

## 2. Project Overview

Wangjialing mine, located in Yuncheng, Shanxi Province, is subordinate to China Coal Huajin Group Co., Ltd., with a mine field area of 119.7 km<sup>2</sup>, industrial reserves of 1.21 billion tons, and recoverable reserves of 777 million tons. The designed production capacity of the mine is 6 million tons per year, and the service life is 92.6 years. The mine field has a simple geological structure and stable coal seam occurrence. The overall structure of the mine field is a monoclinic structure with stratum strike of northeast, dip to west and northwest, accompanied by a wide and gentle anticline fold structure, with numerous and well-developed faults. The No. 12307 working face is located in the west wing of the 123 panel area of Wangjialing Mine. It consists of the 12307 working face belt roadway, the 12307 working face return airway, the 12307 working face open cut, the 12307 working face measure roadway and related bypasses and chambers. Among them, the 12307 return

airway is located 11.4 m south of the 12309 belt roadway (the middle of the lane), and the isolation coal pillar is 6.0 m. The 12307 belt roadway is located 307.9 m south of 12307 return airway (centering in the roadway), and the roadway length is 1475.9 m and section size is  $5.6 \times 3.55$  m. The 12307 working face open cut is located at 1425.5 m west of the 2# coal central auxiliary transportation road (the middle of the roadway), and the working face mining length is 1321.4 m. The 12307 working face roadway layout is shown in Figure 1.

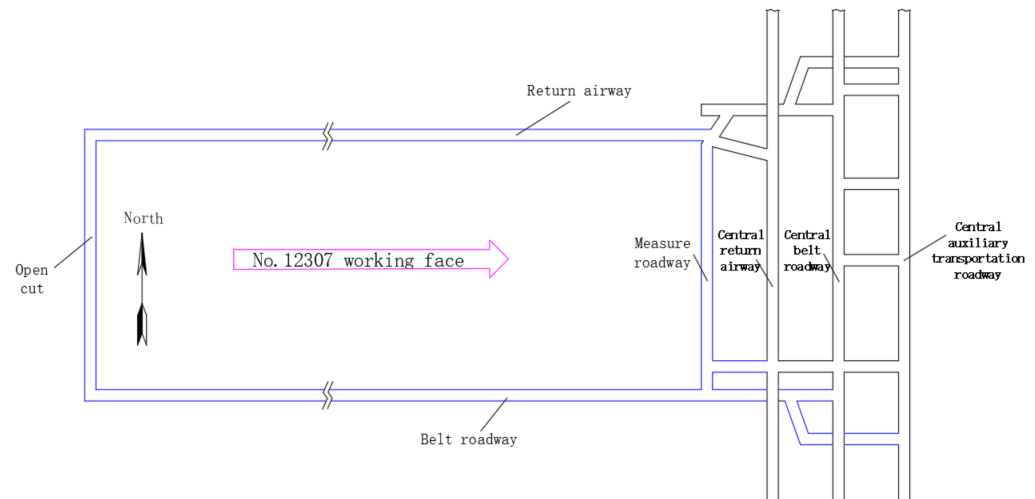


Figure 1. Layout plan of working face.

### 3. Geomechanical Parameters and Distribution Characteristics of the Surrounding Rock of the Roadway

In order to understand the geomechanical parameters and distribution characteristics of roadway-surrounding rock in the Wangjialing coal mine, a representative site was selected as a measurement point for in situ stress measurement, testing the strength of the surrounding rock, and observing the borehole structure to provide a geological basis for determining a reasonable cutting path.

#### 3.1. Ground Stress

Using the coal mine underground SY-56-type small aperture water fracturing ground stress test device, the first measurement point was arranged at 1050 m along the 12322 return air lane of the 2# coal seam, and the second measurement point and the third measurement point were arranged at 50 m and 100 m along the 12307 belt roadway respectively; the location of the measurement point is shown in Figure 2, and the ground stress test results are shown in Table 1 below. In the table:  $H$  is the difference between the measured point burial depth;  $\sigma_v$ ,  $\sigma_H$ ,  $\sigma_h$ ,  $\Delta\sigma$  are the vertical stress, the maximum horizontal principal stress, the minimum horizontal principal stress, and the difference between the maximum and minimum horizontal principal stresses;  $k$ ,  $k_1$ ,  $k_2$  are the ratio of the average principal stress, the maximum horizontal principal stress, the minimum horizontal principal stress and the vertical stress;  $k_3$  is the ratio between the maximum horizontal principal stress and the minimum horizontal principal stress; and the  $\alpha$  is the direction of the maximum horizontal principal stress.

According to Table 1:

- (1) The maximum horizontal principal stress of the first measurement point is 14.01 MPa, the minimum horizontal main stress is 7.48 MPa, and the vertical stress is 10.43 MPa. The maximum horizontal principal stress of the second measuring point is 12.19 MPa, the minimum horizontal principal stress is 6.22 MPa, and the vertical stress is 10.28 MPa. The maximum horizontal principal stress of the third measuring point is 11.89 MPa, the minimum horizontal principal stress is 6.61 MPa, and the vertical stress is 10.46 MPa. The measured regional data are relatively consistent; the maximum horizontal princi-

pal stress is 14.01 MPa, and the maximum value of the minimum horizontal principal stress is 7.48 MPa, but the difference between the maximum and minimum horizontal principal stress is large, and the horizontal stress distribution has obvious directionality. In terms of magnitude, the stress field of the 2# coal seam belongs to the medium stress value area.

- (2) The maximum horizontal principal stress of the measuring point is greater than the vertical stress, the minimum horizontal principal stress is the minimum principal stress, and the type of stress field in the measured area is  $\sigma_H > \sigma_V > \sigma_h$  type stress field. Relevant studies have shown that the maximum horizontal principal stress has a greater impact on the roof and floor of the roadway than on the two sides of the roadway, while the vertical stress mainly affects the stress and deformation of the two sides of the roadway.
- (3) The maximum horizontal principal stress direction of the three measurement points is  $N78.2^\circ W$ ,  $N63.5^\circ W$ ,  $N56.0^\circ W$ , and the dominant direction of the maximum horizontal main stress is the NWW direction.

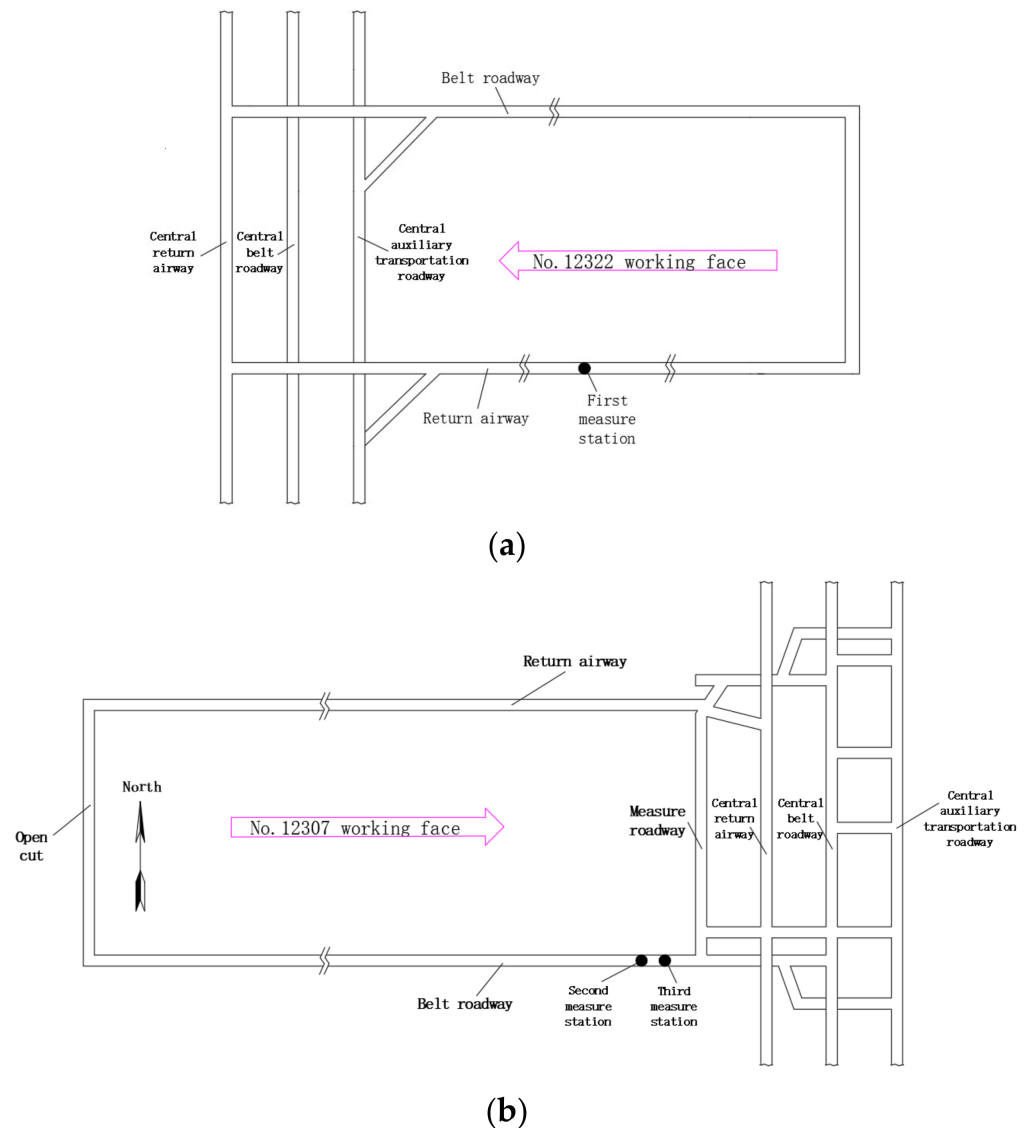


**Figure 2.** Schematic diagram of the location of the measurement point. (a) First measure station; (b) second and third measure station.



### 3.3. Surrounding Rock Strength

The drilling touch method was used to test the strength of surrounding rock in the 12307 belt roadway. One 10 m deep borehole was arranged in a horizontal direction from the middle of the vertical roof and the middle of the roadway side respectively. The wqcz-56 surrounding rock strength test device was used to measure the compressive strength of the coal and rock mass in different layers within 10 m of the roof and the two sides. Figure 4 shows the strength test results of surrounding rock of the 12307 belt roadway.

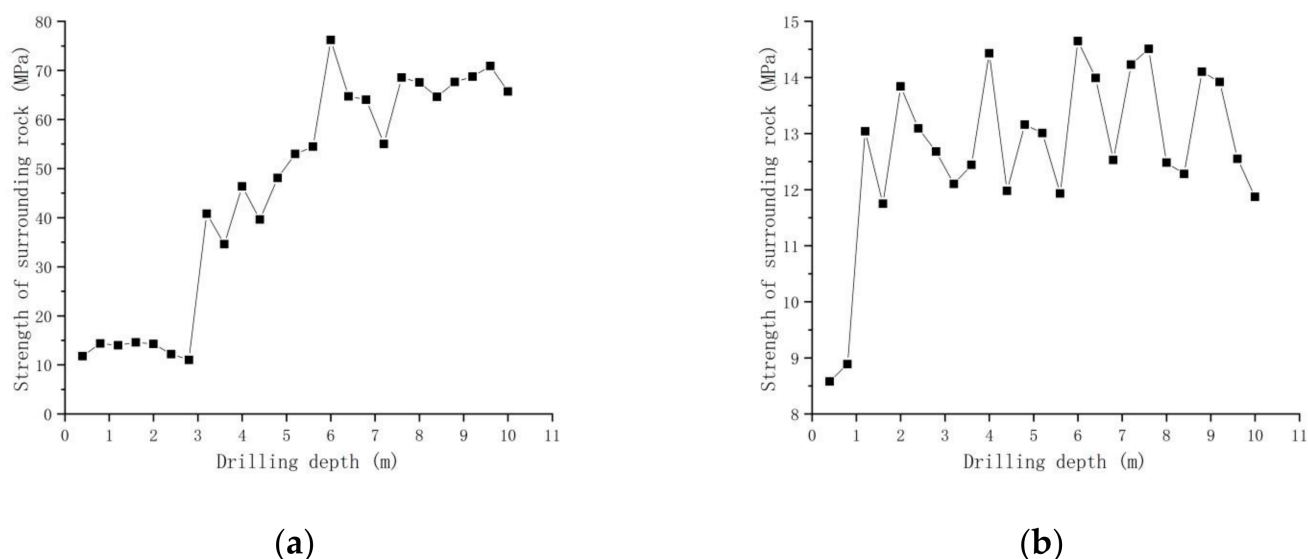


**Figure 4.** 12307 Gelatin Lane surrounding rock strength test result curve. (a) Roadway roof; (b) roadway side.

From Figure 4, we can conclude:

- (1) The top coal is within 3.2 m above the roof of the roadway, the compressive strength is between 11 and 15 MPa, and the average compressive strength is 13.18 MPa, which is small. The range of 3.2~5 m is sandy mudstone, the compressive strength is 34~50 MPa, and the average compressive strength is 41.9 m. In the range of 5 to 10 m, it is fine-grained sandstone, the compressive strength is 50~80 MPa, and the average compressive strength is 64.71 MPa, which is relatively strong. It can be seen that even in the relatively hard and intact rock, the strength of the surrounding rock will fluctuate significantly.
- (2) Whether it is the roof or the two sides, the strength difference and fluctuation of surrounding rock are obvious. Notably, when the hole depth is small, the strength of the surrounding rock will increase drastically. The strength of roof surrounding rock increases from 11 Mpa to 40 MPa, and the strength of roadway-surrounding rock rises from 9 Mpa to 13 Mpa. The obvious difference and fluctuation may be caused by the influence of structural planes such as joints, fissures and weak interlayer, damage to the roadway surface and deep surrounding rock due to excavation, which reduces or loses the strength of surrounding rock, and the different properties between rock strata.

## 4. Numerical Simulation

There are two numerical simulation methods of rock particle physics and Mechanics: laboratory scale discrete element numerical inversion method and engineering scale finite element method [26]. The finite element method is the most widely used method, whereas the discrete element method has become popular in recent years [27]. FLAC 3D software is between the two methods. It adopts the finite separation method, which is mainly a rock mechanics calculation program developed for geotechnical engineering applications.

It can be used to study and analyze the law of surrounding rock activity and roadway stability in the mining process, involving a series of complex mechanical problems, such as rock mass mechanical characteristics, surrounding rock pressure, support-surrounding rock interaction relationship, time-space relationship between roadway and working face and so on. Therefore, this paper used FLAC 3D numerical software for numerical simulation analysis.

4.1. Cutting Path Analysis

The section of coal roadway is formed by the cutting head of roadheader through the process of point, line and surface cutting. The cutting path of the cutting head of the roadheader has a great impact on the disturbance times of the surrounding rock, the stability of the surrounding rock of the roadway in the empty roof area and the actual efficiency of the roadheader. Research on a reasonable and efficient cutting path is of great significance to improving the tunneling speed of the coal roadway. At present, the common cutting paths are “snake” and “loop” cutting paths, as shown in Figures 5 and 6 below.

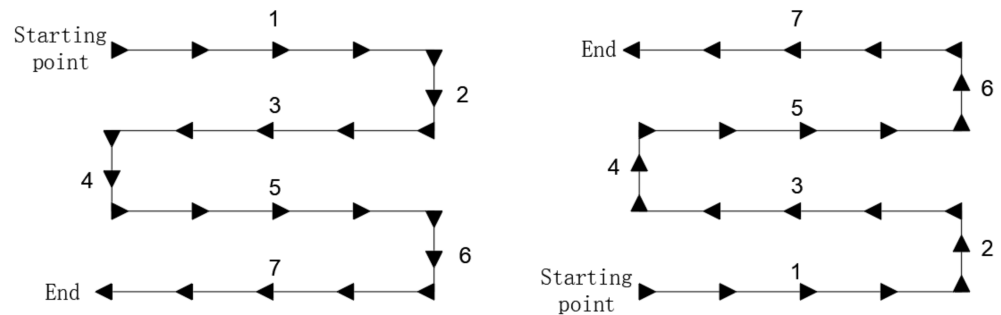


Figure 5. “snake” cutting path track diagram.

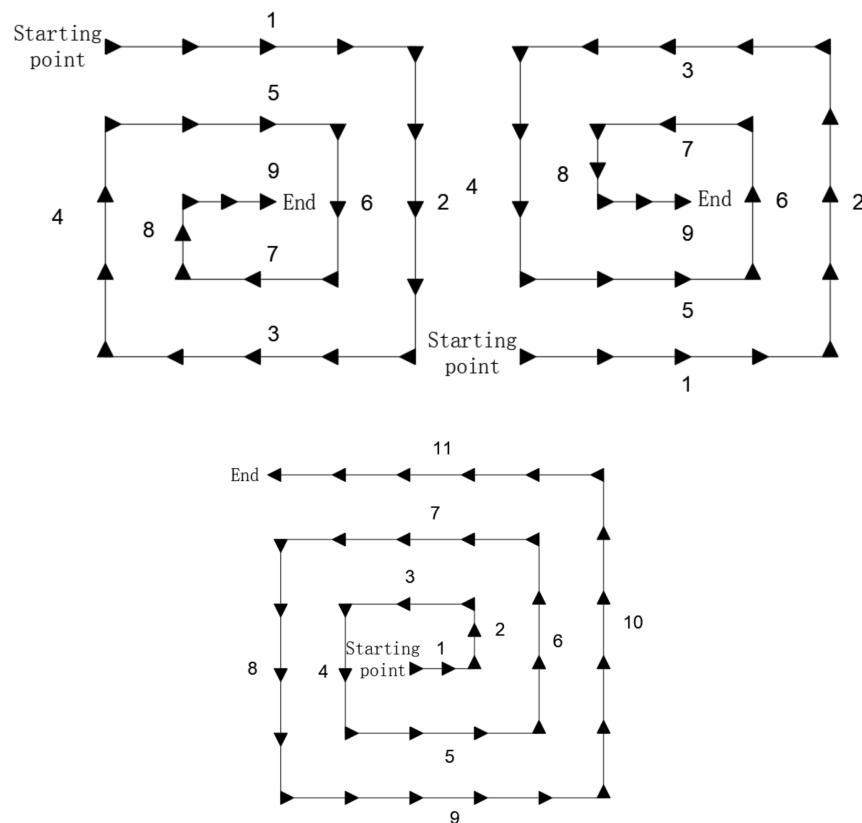


Figure 6. “loop” cutting path track diagram.

#### 4.2. Simulation Model Building

According to the St. Venant principle and combined with the experience of previous construction, the impact area of the roadway excavation is 3~5 times the radius of the roadway [28]. Therefore, the dimensions of the simulation model could be determined: 95 m in the  $x$ -axis direction, 50 m in the  $y$ -axis direction, and 50 m in the  $z$ -axis direction. The simulation is shown in Figure 7. Based on the comprehensive column diagram of the 12307 belt roadway borehole and combined with the results of the geomechanical testing of the surrounding rock, the rock mechanical parameters of the numerical simulation could thus be obtained. The rock mechanics parameters are shown in Table 2. The buried depth of the 12307 belt roadway is 428 m, and the geological stress test results (Serial number 2 in Table 1) are as follows: the vertical stress is 10.28 MPa, the maximum horizontal principal stress is 12.19 MPa, and the minimum horizontal principal stress is 6.22 MPa. The above stress values were applied to the FLAC numerical model as boundary conditions and then calculated to equilibrium to simulate the original rock stress before excavation. The Mohr–Coulomb yielding criterion was used for the numerical simulation.

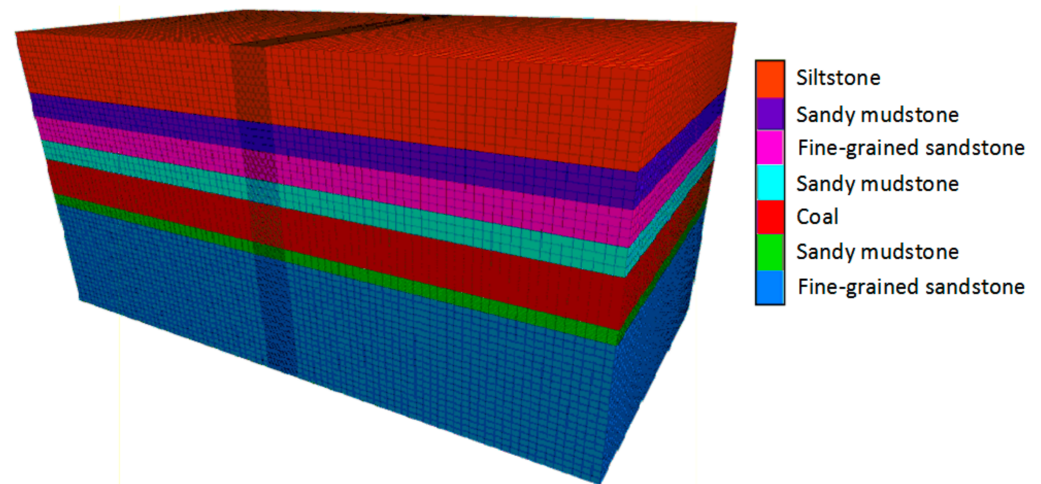


Figure 7. Numerical calculation model.

Table 2. Physical and mechanical parameters of simulated surrounding rock.

Serial Number	Bulk Modulus /GPa	Internal Friction Angle /°	Tensile Strength /Mpa	Density kg/m <sup>3</sup>	Shear Modulus /GPa	Cohesion /MPa	Lithology
1	5.94	32	5.52	2700	4.05	1.53	Siltstone
2	3.65	27	4.63	2500	1.82	1.35	Sandy mudstone
3	10.35	36	6.84	2800	7.74	3.15	Fine-grained sandstone
4	3.7	27	4.54	2500	1.77	1.35	Sandy mudstone
5	1.35	23	3.00	1400	0.63	0.72	Coal
6	3.6	29	4.74	2500	1.89	1.35	Sandy mudstone
7	10.35	36	6.34	2800	7.74	3.15	Fine-grained sandstone

#### 4.3. Analysis of Simulation Results

##### 4.3.1. Snake Path

In the process of coal roadway excavation, the first way for the roadheader to cut the roadway section is to advance the cutting head from top to bottom, then cut continuously from left to right, reach the right side of the roadway, and then cut continuously from right to left; that is, the cutting path is “snake”. We collected data after finite element simulation of the cutting path, and analyzed the variation characteristics of roadway-surrounding rock stability. The displacement evolution law of roadway-surrounding rock is shown in Figure 8.

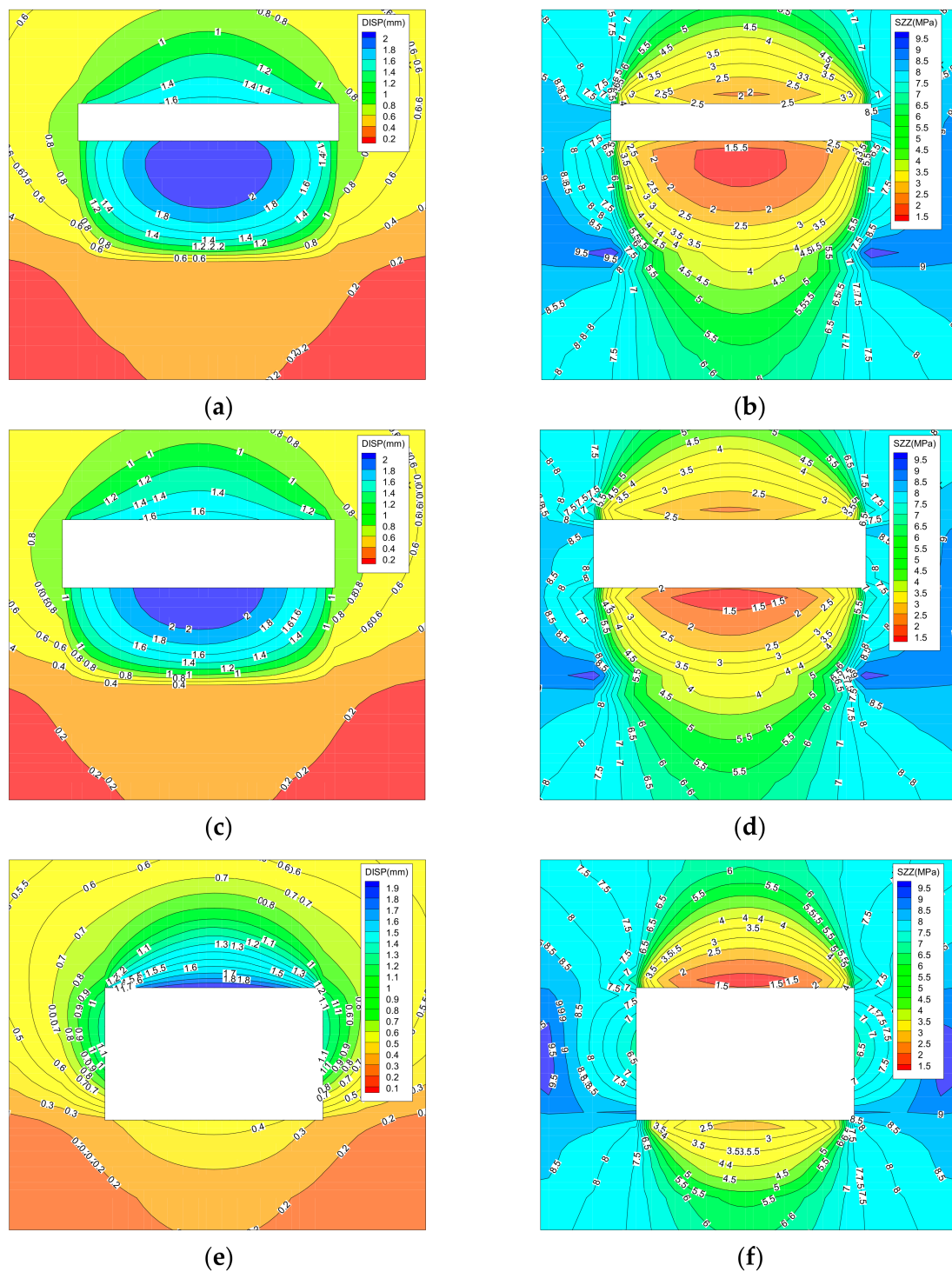


**Figure 8.** Section diagram of displacement (left) and stress (right) distribution of “snake” cutting path from top to bottom. (a,b) The first truncation; (c,d) the second truncation; (e,f) the fifth cutting.

The second way is to advance the cutting head from bottom to top, and then continue cutting from left to right to reach the right side of the roadway, and then continue cutting from right to left. The cutting path also presents a “snake shape”. We simulated the cutting path, collected data and analyzed the variation characteristics of roadway-surrounding rock stability. The displacement evolution law of roadway-surrounding rock is shown in Figure 9.

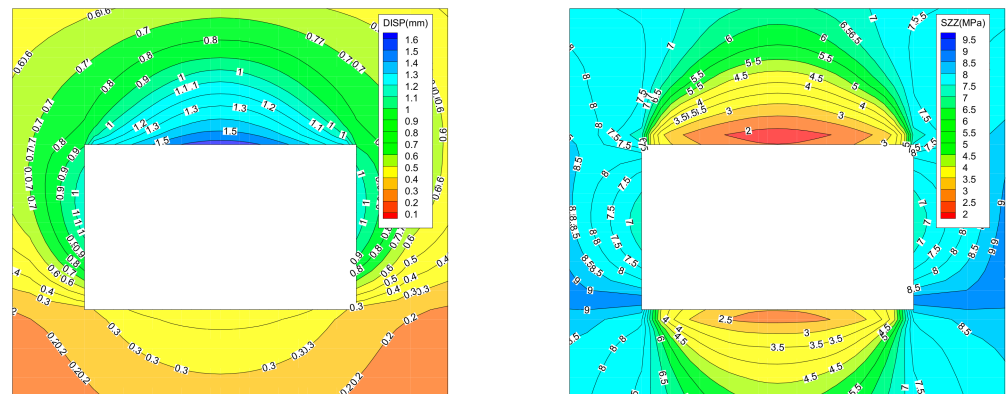


**Figure 9.** Section diagram of displacement (left) and stress (right) distribution of “snake” cutting path from bottom to top (the fifth cutting).

From the displacement nephogram of cutting section in Figures 8 and 9, it can be seen that the range of maximum displacement of roadway roof increases with the increase in cutting times, and the roof displacement reaches the maximum when roadway cutting and forming takes place. The displacement of the coal body in the middle of the roadway section is the largest, which proves that the coal body here is broken and soft, and it is easy for the cutting head to enter.

It can be seen from the stress distribution diagram of the cutting section in Figures 8 and 9 that the stress contour of the roadway floor gradually increases in an elliptical shape, and the range of the low stress area gradually increases with the increase in the cutting times. The stress in the coal to be cut in the roadway does not change significantly with the increase in the cutting times, and the range of the low stress area in the sidewall gradually expands with the increase in the cutting times.

To sum up, after the coal roadway was formed, the maximum displacement of roadway roof in the “snake” cutting path cut from bottom to top increased to 160 mm, which was smaller than the 190 mm of maximum displacement of roadway roof seen in the top-down cutting path. The reason for this was that the top plate was formed earlier when cutting from the top to the bottom. As the number of downward cuts increased, each cut caused disturbance to the roof plate. This caused an increase in the displacement of the roof plate, which made it difficult to control the roof plate, and the quality of the roadway forming was poor.

#### 4.3.2. Loop Path

In this process of coal roadway excavation, the cutting head cuts from left to right along the peripheral contour of the roadway design section from the roof, and then cuts from top to bottom, cutting the section in a clockwise motion. Alternately, it cuts from the bottom plate first from left to right, and then from bottom to top, cut the section in counterclockwise. These cutting path are “clockwise loop” and “reverse loop” respectively. The finite element simulation was carried out respectively, and then the data were collected to analyze the stress and deformation distribution characteristics of the surrounding rock of the roadway. The vertical stress and deformation law of the surrounding rock along the “clockwise loop” cutting path is shown in Figure 10.

The evolution law of vertical stress and displacement of surrounding rock in the “reverse loop” cutting path is shown in Figure 11 (because the picture occupies too much space and is opposite to the “forward loop” cutting path, the cloud map of stress and displacement distribution of surrounding rock in the first eight cuts is omitted).

As can be seen from the displacement nephogram of Figures 10 and 11:

- (1) During “clockwise loop” cutting, the maximum displacement of the roof after the first cutting is 160 mm, the maximum displacement of the design roadway section center is 200 mm, the maximum displacement of the roof after the second cutting is 180 mm,

and the maximum displacement of the design roadway section center is 220 mm. This is due to the increase in the roof displacement caused by the increase in the forming displacement of the right side after the second cutting. After the third cutting, the roadway floor is formed, and the maximum displacement of the floor is 40 mm, while the displacement of the right upper roof changes little.

- (2) During “reverse loop” cutting, the roadway floor is formed after the first cutting, and the floor displacement is small. The maximum displacement in the coal to be cut reaches 200 mm, which is because the roadway floor is fine-grained sandstone and the floor deformation is small. After the second cutting, the forming displacement of the right upper increases to 80 mm, and the displacement of the bottom plate changes less. After the third cutting, the roof is formed, the displacement of the roof increases to 140 mm, and the maximum displacement of the right side increases to 100 mm. This is because when the roof is formed, the support stress of the right side increases, and the deformation increases.
- (3) Whether it is “clockwise loop” or “reverse loop” cutting, the left side is formed after the fourth cutting, the displacement of roadway roof changes less, and the displacement of coal to be cut increases. This is because the coal to be cut has been broken after the third cutting. At this time, the left side has played the role of supporting the roof, and the displacement of left side is generated. After the fourth cutting, because the coal to be cut has no force on the surrounding rock of the roadway, with the increase in cutting times, the displacement and deformation of the surrounding rock of the roadway changes less, and the displacement of the coal to be cut changes greatly. At this time, the coal to be cut is relatively broken and easy to cut.

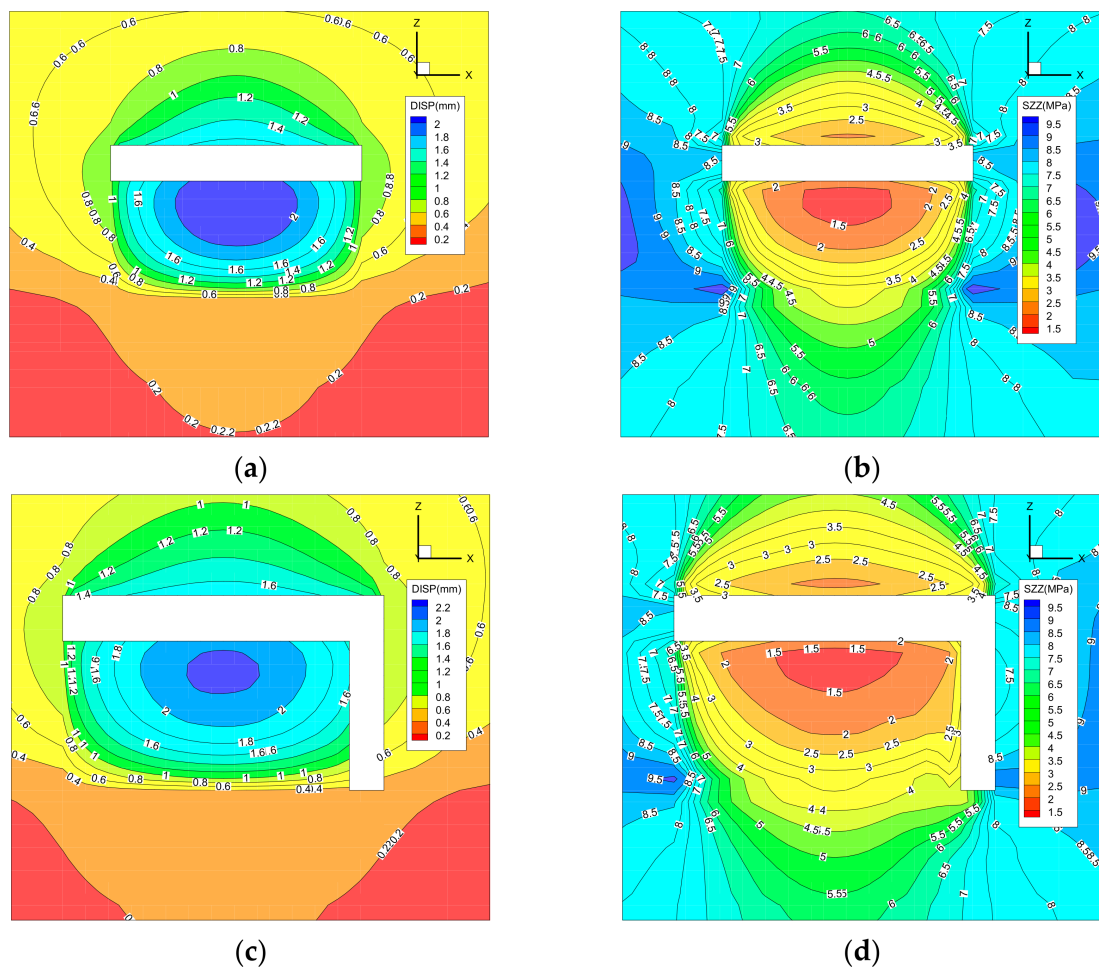
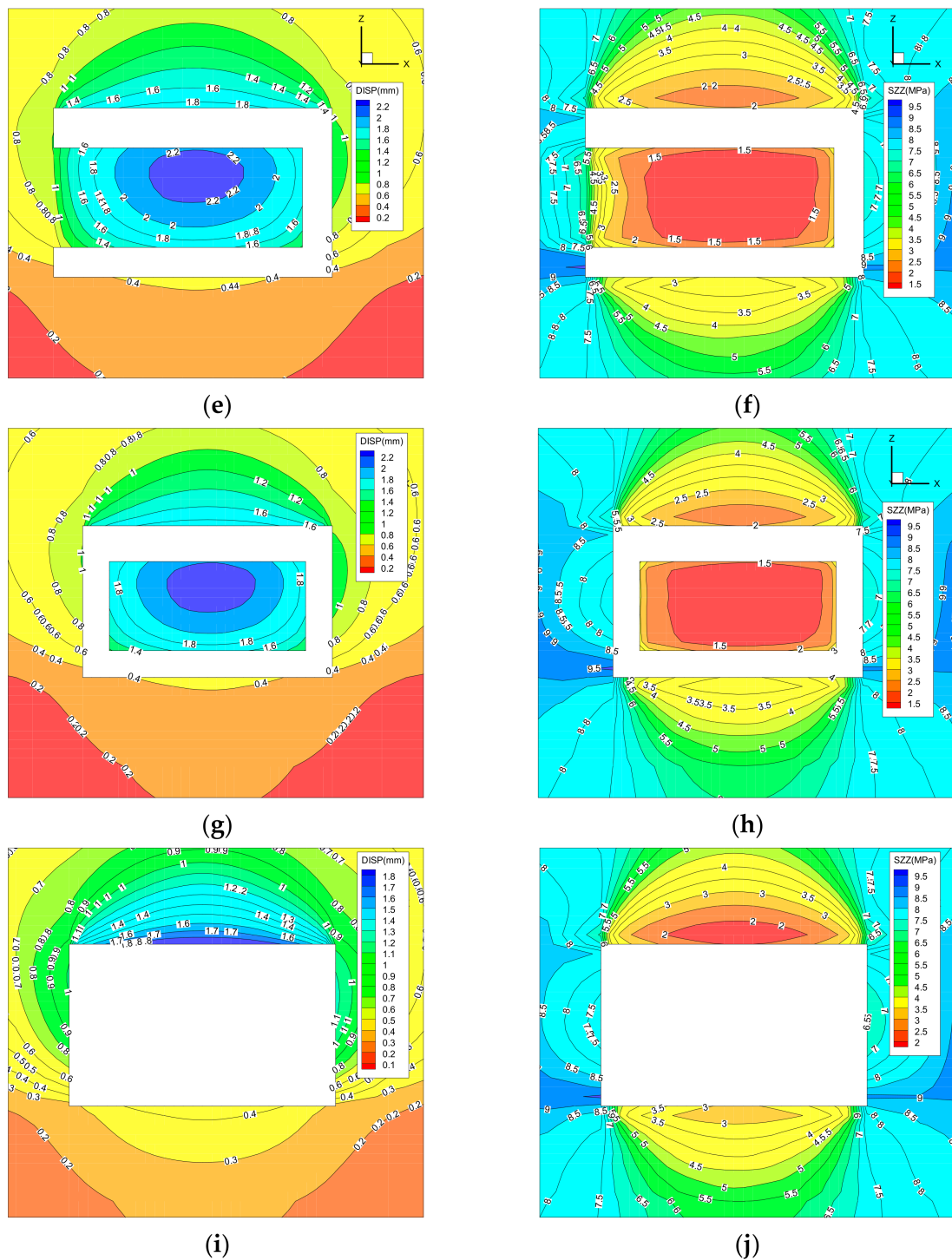


Figure 10. Cont.



**Figure 10.** Displacement of “clockwise loop” cutting path (left), stress (right) distribution clouds. (a,b) The first cutting; (c,d) the second cutting; (e,f) the third cutting; (g,h) the fourth cutting; (i,j) the ninth cutting.

From the stress nephogram in Figures 10 and 11, it can be seen that after the first cutting the roof stress is released, and the stress in the coal to be cut is also released and reduced. After the second cutting, the right side is formed, the stress concentration area moves to the deep part of the surrounding rock, and the shallow stress decreases. The stress of the coal body to be cut continues to release, and the range of the low stress area continues to expand. After the third cutting, the roadway floor is formed, the range of low

stress area in the shallow part of the floor is expanded, the low stress area of the coal body to be cut continues to expand, the left side stress concentration area moves to the deep part, and the shallow stress is reduced. After the fourth cutting, because the coal to be cut has no force on the surrounding rock of the roadway, the stress change of the surrounding rock of the roadway is not obvious with the increase in cutting times.

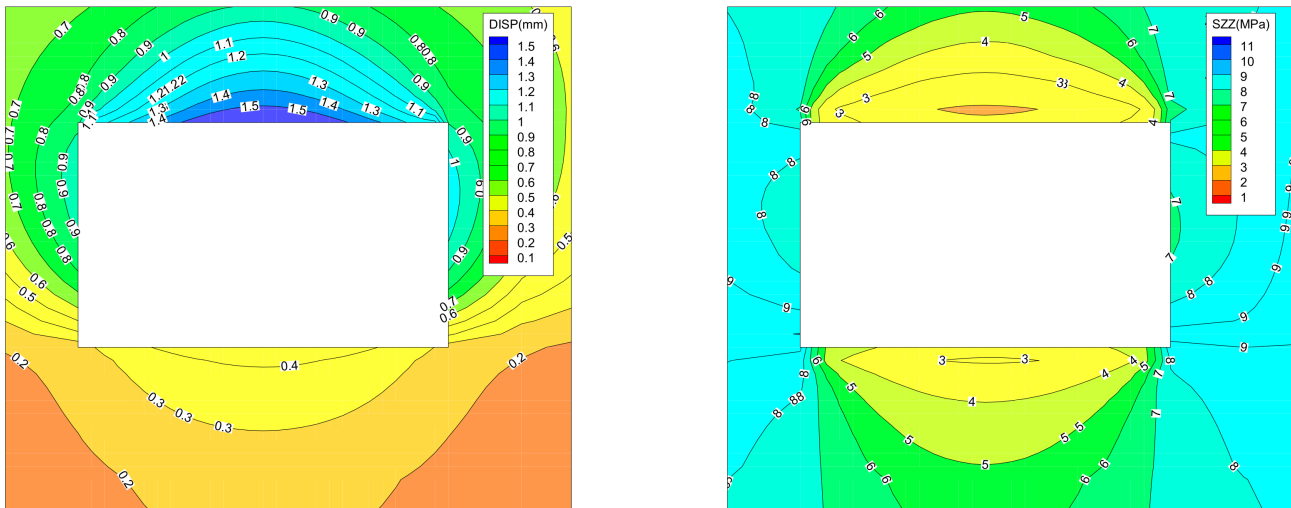


**Figure 11.** Displacement of “reverse loop” truncation path (left), stress (right) distribution clouds (the ninth truncation).

The cutting head feeds from the middle of the roadway design section, cuts the roadway counterclockwise from right to left, then from top to bottom, and finally forms the design section. The vertical stress and displacement evolution law of the surrounding rock of the “loop” cutting path of the middle feed is shown in Figure 12 (the same as omitting the cloud diagram of the first eight cutting stresses and displacements).

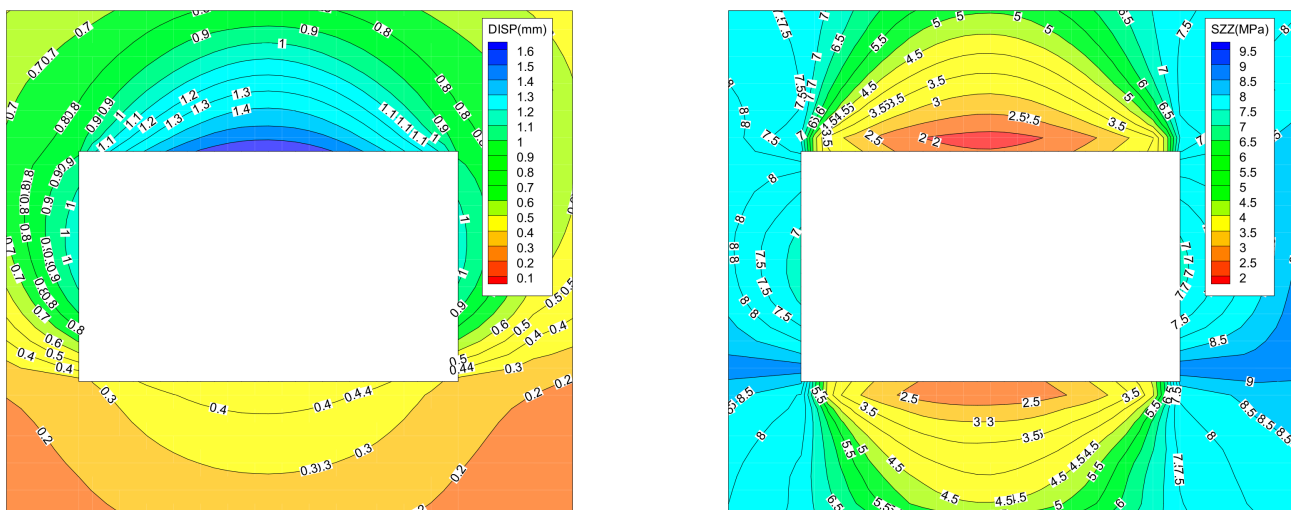


**Figure 12.** Nephogram of displacement (left) and stress (right) distribution of “loop” cutting path of intermediate feed (the ninth truncation).

It can be seen from the cloud map of displacement distribution (left of Figure 12) that the feed position of cutting head is the middle position of roadway section. During the first five cuts, the displacement of roadway-surrounding rock increases slowly with the increase in cutting times. After the sixth cutting, the left side is formed, and the displacement of the left side increases to 80 mm. After the seventh cutting, the bottom plate is formed



support → withdraw the anchor drill truck, enter the roadheader and cut the coal into the next cycle. As shown in Figure 14 below.

**Table 3.** Table of main equipment for the tunneling.

Serial Number	Device Name	Specifications	Quantity
1	Roadheader	EBZ-220Z	1
2	Bolt drilling rig	CMM2-25Z	1
3	Belt conveyor	DSJ100/80/2 × 200	1
4	Self-moving tail of belt conveyor	DWZY1000/1200(A)	1
5	Belt Loader	DZQ100/100/40	1
6	Dust removal fan	KCS-700D	1
7	Bolt machine	MQT-130	4
8	Air leg rock drill	YT-28	4
9	Local ventilator	FBD№7.5/2 × 45 kw	2

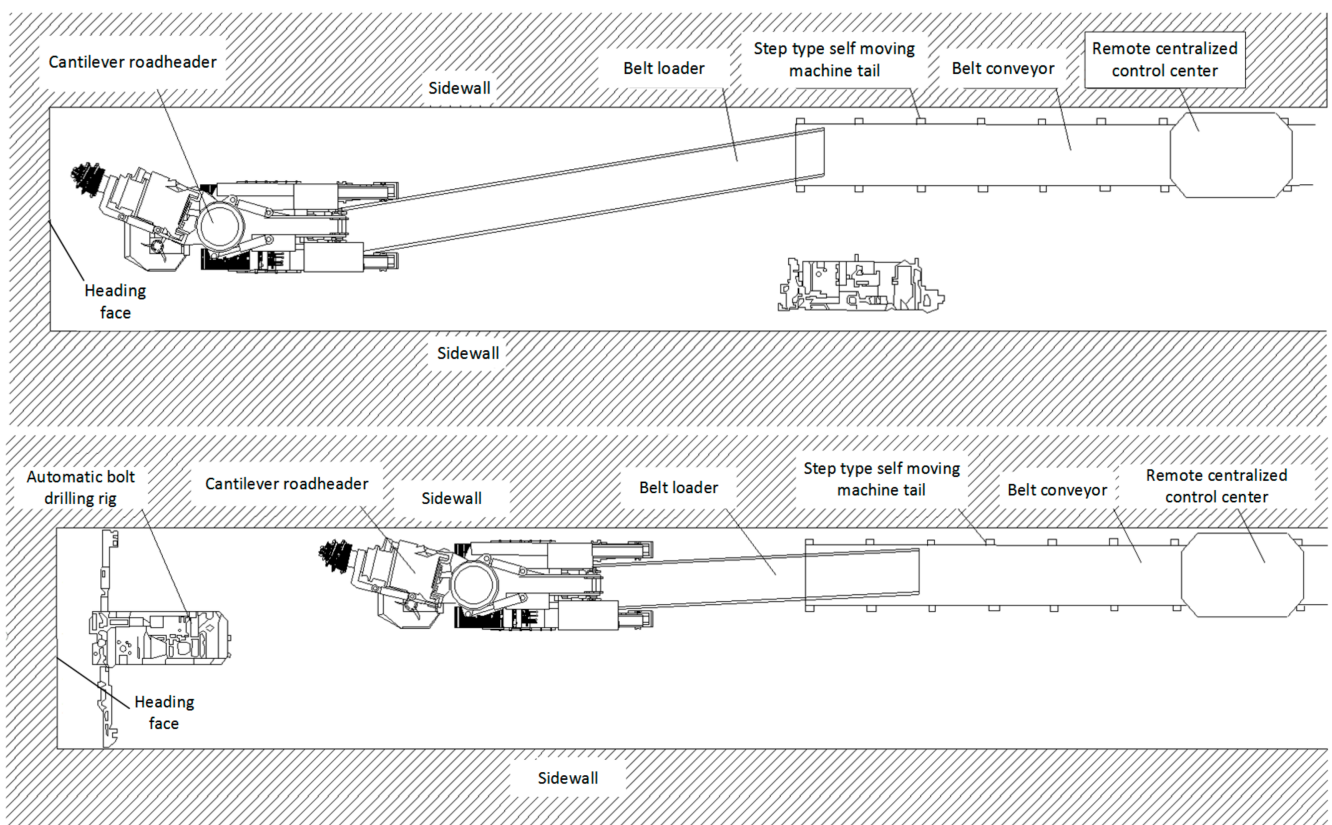


**Figure 14.** Construction process flow chart.

### 5.2. Implementation Effects

According to the actual test on site, the roadway cutting and forming effect of scheme 1 (Figure 13a) was good (as shown in Figure 15), and the roadheader could remain stable in the cutting process. On the other hand, after communicating with the roadheader driver, the cutting path in scheme 1 was deemed to be more suitable for their operation than the cutting path in scheme 2. To sum up, cutting scheme 1 was selected as the cutting path of the roadheader.

The cutting head was drilled from 3150 mm away from the left side of the roadway. When the cutting arm swung from right to left to 350 mm away from the left side, the cutting arm swung from bottom to top. After entering the coal, it swung from left to right to cut along the “snake” cutting route. Finally, the cutting arm swung from top to bottom to the roadway bottom plate to ensure the forming effect of the roadway. The second cutting

was carried out by adjusting the position of the roadheader. The cutting head was drilled from 1750 mm away from the right side of the roadway. When the cutting arm swung from left to right to 350 mm away from the right side, the cutting arm entered an excavation path from bottom to top, and then cut along the “snake” cutting road line as shown in scheme 1 of Figure 13a. The whole cutting process was parallel to coal discharging and material preparation, which took 34 min. The time consumption of each process is shown in Table 4 below.



**Figure 15.** The cut section of the roadway.

**Table 4.** Time-consuming table of each process.

Process	Time/Min
Pre-operation inspection	1
Incoming machine	2
Bottom cutting	1
Cutting the left side	6
Cleaning and transporting float coal	2
Repair roof, left shoulder socket	2
Repair the bottom feet of left side	1
Cleaning and transporting float coal	2
Adjusting machine	2
Cutting the right side	5
Cleaning and transporting float coal	2
Repair roof, right shoulder socket	1
Repair the bottom feet of right side	2
Cleaning and transporting float coal	2
Return machine	2
Power outage locking	1
Total	34

## 6. Conclusions

Based on the engineering background of the 12307 belt roadway in Wangjialing coal mine, this paper studied the cutting path design of roadways driven by a cantilever roadheader.

- (1) Representative sites were selected as measurement points to observe the geomechanical parameters and distribution characteristics of the surrounding rocks in the roadway of Wangjialing Coal Mine, so as to provide a parameter basis for numerical simulation.

- (2) Based on the observation results, a numerical simulation model was established to study the distribution law of stress meter displacement of roadway-surrounding rock under “snake” and “loop” cutting paths. The simulation results showed that the bottom-up “snake” cutting path and “reverse loop” cutting path were the best.
- (3) Combined with the simulation results and the actual situation of the 12307 belt roadway, two cutting schemes were designed (Figure 14). The field test showed that cutting scheme 1 was more conducive to the formation of the roadway, and the single cycle cutting took 34 min, which not only ensures the formation effect of the roadway, but also improves the tunneling efficiency and safety. Therefore, combined with the actual situation of roadway excavation, the numerical simulation analysis method can be used to design the cutting path during roadway excavation.

**Author Contributions:** C.H., Y.Z., R.Y. and L.W. designed the study and experiment; C.H., B.Z. and Z.X. collected the data; C.H., R.Y., L.W. and Z.X. conducted the data analysis; R.Y., L.W. and B.Z. provided the statistical methods; C.H., X.F., R.Y. and Z.X. drafted the paper; C.H., Y.Z. and X.F. edited the paper. All authors have read and agreed to the published version of the manuscript.

**Funding:** This research was funded by the National Natural Science Foundation of China (No. 51874276) and the Fundamental Research Funds for the Central Universities (No. 2020ZDPY0209).

**Institutional Review Board Statement:** Not applicable.

**Informed Consent Statement:** Not applicable.

**Data Availability Statement:** All data and code used or analyzed in this study are available from the corresponding author on reasonable request.

**Acknowledgments:** The authors thank the editor and three anonymous reviewers of the paper. Their constructive suggestions and comments have considerably improved the quality of the paper.

**Conflicts of Interest:** The authors declare no conflict of interest.

## References

1. Milici, R.C.; Flores, R.M.; Stricker, G.D. Coal resources, reserves and peak coal production in the United States. *Int. J. Coal Geol.* **2013**, *113*, 109–115. [[CrossRef](#)]
2. Wang, J. Development and prospect on fully mechanized mining in Chinese coal mines. *Int. J. Coal Sci. Technol.* **2014**, *1*, 253–260. [[CrossRef](#)]
3. Tang, B.; Cheng, H.; Tang, Y.; Zheng, T.; Yao, Z.; Wang, C.; Rong, C. Supporting Design Optimization of Tunnel Boring Machines-Excavated Coal Mine Roadways: A Case Study in Zhangji, China. *Processes* **2020**, *8*, 46. [[CrossRef](#)]
4. Kramadibrata, S.; Simangunsong, G.M.; Widodo, N.P.; Wattimena, R.K.; Tanjung, R.A.; Wicaksana, Y. Rock excavation by continuous surface miner in limestone quarry. *Geosyst. Eng.* **2015**, *18*, 127–139. [[CrossRef](#)]
5. Dalgic, S. Influence of weak rocks on excavation of the Beykoz Tueel, Turkey. *Eng. Geol.* **2000**, *58*, 137–148. [[CrossRef](#)]
6. Choi, S.O.; Shin, H.S. Stability analysis of a tunnel excavated in a weak rock mass and the optimal supporting system design. *Int. J. Rock Mech. Min. Sci.* **2004**, *41*, 876–881. [[CrossRef](#)]
7. Menezes, P.L.; Lovell, M.R.; Avdeev, L.V.; Higgs, C.F., III. Studies on the formation of discontinuous rock fragments during cutting operation. *Int. J. Rock Mech. Min.* **2014**, *71*, 131–142. [[CrossRef](#)]
8. Menezes, P.L. Influence of cutter velocity, friction coefficient and rake angle on the formation of discontinuous rock fragments during rock cutting process. *Int. J. Rock Mech. Min. Sci.* **2017**, *90*, 3811–3827. [[CrossRef](#)]
9. Menezes, P.L. Influence of rock mechanical properties and rake angle on the formation of rock fragments during cutting operation. *Int. J. Adv. Manuf. Technol.* **2017**, *90*, 127–139. [[CrossRef](#)]
10. Bilgin, N.; Demircin, M.A.; Copur, H.; Balci, C.; Tuncdemir, H.; Akcin, N. Dominant rock properties affecting the performance of conical picks and the comparison of some experimental and theoretical results. *Int. J. Rock Mech. Min. Sci.* **2006**, *43*, 139–156. [[CrossRef](#)]
11. Fowell, R.J. The mechanics of rock cutting. In *Comprehensive Rock Engineering*; Hudson, J.A., Ed.; Elsevier: Pergamon, Turkey; Oxford, UK, 1993; pp. 155–175.
12. Deliac, E.P. Theoretical and practical rules for mechanical rock excavation. In *Comprehensive Rock Engineering*; Hudson, J.A., Ed.; Elsevier: Pergamon, Turkey; Oxford, UK, 1993; pp. 177–227.
13. Acaroglu, O.; Ergin, H. The effect of cutting head shapes on roadheader stability. *Min. Technol.* **2005**, *114*, 140–146. [[CrossRef](#)]
14. Acaroglu, O.; Ergin, H. A new method to evaluate roadheader operational stability. *Tunn. Undergr. Space Technol.* **2006**, *21*, 172–179. [[CrossRef](#)]

15. Ergin, H.; Acaroglu, O. The effect of machine design parameters on the stability of a roadheader. *Tunn. Undergr. Space Technol.* **2007**, *22*, 80–89. [[CrossRef](#)]
16. Salsani, A.; Daneshian, J.; Shariati, S.; Yazdani-Chamzini, A.; Taheri, M. Predicting roadheader performance by using artificial neural network. *Neural Comput. Appl.* **2014**, *24*, 1823–1831. [[CrossRef](#)]
17. Comakli, R.; Kahraman, S.; Balci, C. Performance prediction of roadheaders in metallic ore excavation. *Tunn. Undergr. Space Technol.* **2014**, *40*, 38–45. [[CrossRef](#)]
18. Faradonbeh, R.S.; Salimi, A.; Monjezi, M.; Ebrahimabadi, A.; Moormann, C. Roadheader performance prediction using genetic programming (GP) and gene expression programming (GEP) techniques. *Environ. Earth Sci.* **2017**, *76*, 584. [[CrossRef](#)]
19. Seker, S.E.; Ocak, I. Performance prediction of roadheaders using ensemble machine learning techniques. *Neural Comput. Appl.* **2019**, *31*, 1103–1116. [[CrossRef](#)]
20. Wang, F.; Zhang, C.; Wei, S.; Zhang, X.; Guo, S. Whole section anchor–grouting reinforcement technology and its application in underground roadways with loose and fractured surrounding rock. *Tunn. Undergr. Space Technol. Inc. Trenchless Technol. Res.* **2016**, *51*, 133–143.
21. Cao, R.; Cao, P.; Lin, H. Support technology of deep roadway under high stress and its application. *Int. J. Min. Sci. Technol.* **2016**, *26*, 787–793. [[CrossRef](#)]
22. Yang, S.Q.; Chen, M.; Jing, H.W.; Chen, K.F.; Meng, B. A case study on large deformation failure mechanism of deep soft rock roadway in Xin’An coal mine. *China Eng. Geol.* **2016**, *217*, 89–101. [[CrossRef](#)]
23. Ding, Y. The current situation of high efficiency and rapid driving system and development of support equipment. *Coal Eng. Coal Eng.* **2020**, *52*, 168–171.
24. Cha, T. Development trend and situation of speed drivage system in coal mine. *Coal Technol.* **2021**, *40*, 30–32.
25. Liu, C.; Jiang, P.; Wang, Z.; Wei, R.; Luo, C.; Guo, J. Research on current situation of rapid driving technology in coal roadway and its assessment method of application effect. *Coal Sci. Technol.* **2020**, *48*, 26–33.
26. Zhang, C.; Zhao, Y.; Bai, Q. 3D DEM method for compaction and breakage characteristics simulation of broken rock mass in goaf. *Acta Geotechnica* **2021**, 1–17. [[CrossRef](#)]
27. Zhang, C.; Zhao, Y.; Han, P.; Bai, Q. Coal pillar failure analysis and instability evaluation methods: A short review and prospect. *Eng. Fail. Anal.* **2022**, *138*, 106344. [[CrossRef](#)]
28. Tsinidis, G.; Pitilakis, K.; Madabhushi, G. On the dynamic response of square tunnels in sand. *Eng. Struct.* **2016**, *125*, 419–437. [[CrossRef](#)]